IgMin Research STEM ISSN: 2995-8067 A Multidisciplinary Open Access Journal

SCIENCE SUBJECT
Computational Chemistry | Spectroscopy | Inorganic Chemistry | Physical Chemistry TOPIC(S)

Article Information

Submitted: June 10, 2024
Approved: June 27, 2024
Published: June 28, 2024

How to cite this article: Bharati M, Singh V, Kripal R. Modeling of Cr^{3+} doped Cassiterite (SnO_2) Single Crystals. IgMin Res. June 28, 2024; 2(6): 484-489. IgMin ID: igmin207; DOI: 10.61927/igmin207; Available at: igmin.link/p207

Keywords: Zero-field splitting; Crystal field; Superposition model; SnO_2; Optical spectroscopy of Cr^{3+} ions

Research Article

Modeling of Cr^{3+} doped Cassiterite (SnO_2) Single Crystals

Maroj Bharati[1], Vikram Singh[1] and Ram Kripal[2]*

[1]Department of Physics, Nehru Gram Bharti (DU), Jamunipur, Prayagraj, India
[2]EPR Laboratory, Department of Physics, University of Allahabad, Prayagraj-211002, India

***Correspondence:** Ram Kripal, EPR Laboratory, Department of Physics, University of Allahabad, Prayagraj-211002, India, Email: ram_kripal2001@rediffmail.com

Abstract

Using the superposition model, the crystal field and zero-field splitting parameters of Cr^{3+} doped cassiterite (tin oxide), SnO_2 single crystals are computed. For calculations, the appropriate locations for Cr^{3+} ions in SnO_2 with distortion are taken into account. The experimental values and the zero-field splitting parameters in theory with local distortion agree fairly well. Using the Crystal Field Analysis Program and crystal field parameters, the optical energy bands for Cr^{3+} in SnO_2 are calculated. The findings indicate that in SnO_2 single crystals, one of the Sn^{4+} ions is replaced by Cr^{3+} ions.

Introduction

When examining the local symmetry of transition ions in crystals, electron paramagnetic resonance, or EPR, is thought to be a crucial tool. The Cr^{3+} ion introduced into different crystals provides good information about the Crystal Field (CF) and zero field splitting (ZFS) parameters [1-4]. When divalent or trivalent impurities are used in place of monovalent ions, it is crucial to compensate for the charge imbalance. In such systems positive ion vacancies fulfill the charge compensation [5]. The optical characteristics of the crystal are impacted by substituted impurities that cause very little structural change. The Superposition Model (SPM) is mostly used for the theoretical estimation of ZFS and CF parameters [6-8]. It is worth mentioning various semiempirical approaches developed for modeling CF parameters (CFPs) based on crystal structure data. Apart from the historically first, Point Charge Model (PCM), other CFP modeling approaches are Superposition Model (SPM), Angular Overlap Model (AOM), and Simple Overlap Model (SOM). These approaches may yield varying results even using the same crystallographic data as input. Various modeling techniques for the analysis and interpretation of EMR data for transition ions at low symmetry sites in crystals have been reviewed [8]. The superposition model was originally developed and applied first to CFPs for lanthanide ions in various crystals and later to CFPs for transition metal ions. Subsequently, its applications have been extended to the semi-empirical parameterization of Zero-Field Splitting Parameters (ZFSPs) and interpretation of EPR spectra for the S-state $3d^5$ and $4f^7$ transition ions. It should be emphasized that out of the semi-empirical approaches applicable for CFPs: PCM, SPM, AOM, and SOM, only SPM is also applicable to ZFSPs. In fact, SPM may be employed independently for modeling both CFPs and ZFSPs, whereas attempts to use PCM for ZFSPs occasionally appear in EMR literature. SPM calculations of CFPs and those of ZFSPs utilize the same mathematical framework [8]. Accurate interpretation of EMR experimental spectra and modeling of ZFSPs is important for proper understanding of spectroscopic and magnetic properties of crystals containing $4f^N$ and $3d^N$ ions. SPM yields calculable predictions for EMR experiments in which transition ions are used as probes to investigate the structure and nature of paramagnetic centers. Modeling using SPM may also help predict characteristics important for potential applications. Hence, SPM calculations of ZFS parameters are of prime importance.

SnO_2 is one of the important semiconducting oxides having desirable qualities such as optical transmittance, mechanical hardness, low resistivity, stability under heat treatment, uniformity, and piezoelectric behavior. This semiconductor, which is of the n-type and has a wide band gap of 3.6 eV at 300 K, is highly iconic and has a wide range of uses. Some of these uses include gas sensors, catalyst supports, dye-sensitized solar cells, supercapacitors, and transparent conducting

ISSN 2995-8067 DOI: 10.61927/igmin207

electrodes [9-13]. Recently, some researchers have added metal or halogen ions to SnO_2 as impurities, changing its surface states, electronic structure, and optical characteristics in the process, which has improved the material's qualities and potential applications [10,14,15]. Moreover, the Cr^{3+}-doped SnO_2 materials are useful in solid-state lighting [16].

EPR study for Cr^{3+} ions in SnO_2 was performed and spin Hamiltonian parameters were evaluated [17]. Sn^{4+} ions have an ionic radius of 0.069 nm, which is marginally greater than Cr^{3+} ions' ionic radius of 0.0615 nm. Hence Cr^{3+} substitutes for one of the Sn^{4+} ions as discussed in [17].

The crystallographic axes (a, b, and c) and the laboratory axes (x, y, and z) are chosen in parallel. The symmetry-adopted axes (magnetic axes) have labels (*X, Y, Z*). The crystallographic c axis is found to correspond with the principal Z axis of the g and D tensors of Cr^{3+} ions.

The superposition model (SPM) analysis of the ZFS and CF parameters for Cr^{3+} ions in SnO_2 single crystal is presented in the current work. Investigating the ZFS parameters, the CF parameters, and the lattice distortion for the Cr^{3+} ions in SnO_2 at octahedral sites is the goal. The Crystal Field Analysis (CFA) computer program and CF parameters are used to determine the optical energy bands for Cr^{3+} ions in SnO_2. The estimated CF and ZFS parameters could both be helpful in later research for obtaining crystals of various scientific and industrial applications.

Crystal structure

SnO_2 belongs to the TiO_2 (Rutile) crystal class, which crystallizes in a space group $P4_2\ 2_1/n\ 2/m\text{-}D_{4h}^{14}$ tetragonal crystal system [18]. The unit cell has the following parameters: a = 0.4737 nm, b = 0.4737 nm, and c = 0.3185 nm. Two nonequivalent Sn^{4+} sites make up the unit cell, and they can be converted into one another by rotating 90^0 around the c-axis. Due to a slight deformation of the SnO_6 octahedra, an orthorhombic local symmetry D_{2h} is formed around the Sn^{4+} site. Figure 1 shows the SnO_2 crystal structure with the Symmetry-Adopted Axis System (SAAS).

The directions of metal-ligand bonds that are mutually perpendicular are the symmetry adopted axes (SAA) or local site symmetry axes. For centers I, the two other axes (X, Y) are perpendicular to the Z axis of SAAS, which is along the metal-ligand bond Sn-O (crystal c-axis) (Figure 1). This suggests that in the SnO_2 crystal, Cr^{3+} takes the place of Sn^{4+} with approximately orthorhombic symmetry. The ionic radius of Cr^{3+} ions (0.0615 nm) is slightly less than that of Sn^{4+} ions (0.069 nm), suggesting that Cr^{3+} ions can, with some distortion, occupy the position of Sn^{4+} ions. The ligands' spherical polar coordinates and the position of the Cr^{3+} ion for center I in SnO_2 are shown in Table 1 [18]. These specifics are employed for Cr^{3+} ion CF and ZFS computations in SnO_2.

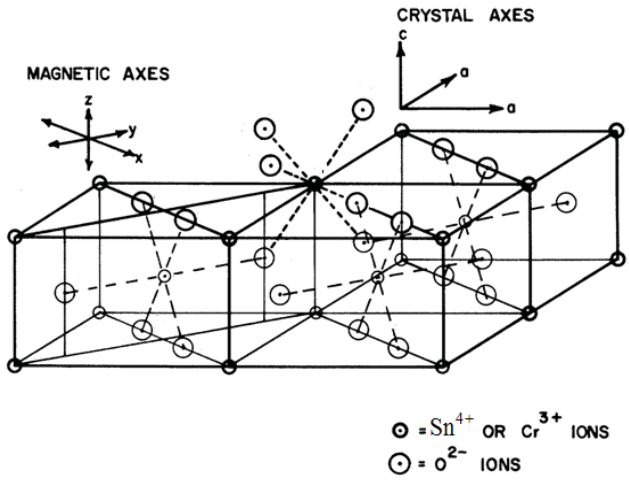

Figure 1: The crystal structure of SnO_2 together with the symmetry-adopted axis system (SAAS).

Table 1: The Cr^{3+} ion's fractional coordinates and the spherical polar co-ordinates (R, θ, ϕ) of ligands (center I) in a single crystal of SnO_2.

Position of Cr^{3+}	Ligands	Spherical polar co-ordinates of ligands		
		$R^{Å}$	Θ^0	Φ^0
ND: Substitutional (0.0000, 0.0000, 0.0000)	O1	2.2772	64.57	45.00
	O2	2.0566	89.91	45.00
	O3	4.2409	67.94	13.44
	O4	4.2409	67.94	76.55
	O5	2.0566	89. 91	-45.00
	O6	2.0566	89.91	-45.00
WD: substitutional Centre I (-0.1662, -0.1185, -0.0022)	O1	3.1712	71.91	41.95
	O2	1.1145	89.47	53.24
	O3	5.0978	71.71	17.74
	O4	4.9672	71.21	68..78
	O5	2.4128	89.92	-21.71
	O6	2.1230	89.91	-71.69

Computations of splitting parameters for zero field

The energy levels of Cr^{3+} ions in crystals are found using the spin Hamiltonian [19-21]:

$$H = H_{Ze} + H_{ZFS} = \mu_B B.g.S + \sum B_k^q O_k^q = \mu_B B.g.S + \sum f_k b_k^q O_k^q \quad (1)$$

Where spectroscopic splitting factor, Bohr magneton, and steady magnetic field are represented by g, μ_B, and B, respectively. *S* represents the effective spin operator and $O_k^q(S_x, S_y, S_z)$ are the extended Stevens operators (ESO) [22,23]; B_k^q and b_k^q are the parameters of ZFS, f_k = 1/3 and 1/60 give the scaling factors for *k* = 2 and 4, respectively. At orthorhombic symmetry sites, the ZFS terms in (1) for the Cr^{3+} ion (S = 3/2) are evaluated as [24,25]:

$$H_{ZFS} = B_2^0 O_2^0 + B_2^2 O_2^2 = \frac{1}{3} b_2^0 O_2^0 + \frac{1}{3} b_2^2 O_2^2 = D(S_z^2 - \frac{1}{3} S(S+1)) + E(S_x^2 - S_y^2) \quad (2)$$

The traditional orthorhombic ZFS parameters *D*, *E* and B_k^q, b_k^q have relations :

$$b_2^0 = D = 3B_2^0, b_2^2 = 3E = B_2^2 \quad (3)$$

ISSN 2995-8067 DOI: 10.61927/igmin207

In ESO notation, the parameters of ZFS for any symmetry utilizing SPM [24,25] are obtained as:

$$b_k^q = \sum_i \bar{b}k\left(R_0\right)\left(\frac{R_0}{R_1}\right)^{tk} K_k^q\left(\theta_i, \varphi_i\right) \quad (4)$$

Where (R_i, θ_i, ϕ_i) present the spherical polar coordinates of the *i*-th ligand. The intrinsic parameters $\bar{b}k$ represent the magnitude of a ligand's k-th rank ZFS contribution at a distance R_i and the coordination factors K_k^q provide the geometrical data. K_k^q for k = 1 to 6 in ESO notation [26] are given in Appendix A1 of [27].

Eq. (4), in terms of the intrinsic parameters $\bar{b}k$, the power-law exponents t_k and the reference distance R_0, provide traditional ZFS parameters, D and E as given below[27,28-30]:

$$b_2^0 = D = \frac{\bar{b}2\left(R_0\right)}{2}\left[\left(\frac{R_0}{R_1}\right)^{t_2} \sum_i\left(3\cos^2\theta_i - 1\right)\right] \quad (5)$$

$$b_2^2 = 3E = \frac{b_2^2}{3}\frac{\bar{b}2\left(R_0\right)}{2}\left[\left(\frac{R_0}{R_1}\right)^{t_2} \sum_i \sin^2\theta_i \cos 2\varphi_i\right]$$

The Sn^{4+} ion site and the interstitial site with a comparable ligand environment are expected to be substituted by the Cr^{3+} ion in SnO_2. The Cr^{3+} ion's local symmetry is orthorhombic. In $LiNbO_3$ having octahedral coordination of Cr^{3+} ion with Cr^{3+}-O^{2-} bond, t_2 = -0.12 and = 2.34 cm^{-1} [31] were taken to compute b_2^0 and b_2^2. Since oxygen serves as a ligand and the Cr^{3+} ion in SnO_2 has distorted octahedral coordination (Figure 1), the b_K^q in the current study is established using $\bar{b}_2(R_0)$ = 2.34 cm^{-1} and t_2 = -4.173 for the center I.

The spherical polar coordinates of ligands and the Cr^{3+} ion's location as shown in Table 1 are considered for computation. The traditional ZFS parameters, D and E of Cr^{3+} ion in a single crystal of SnO_2 are calculated using Eq. (5). The reference distance R_0 = 0.200 nm is used [32] to find the ZFS parameters, and the values are: |D| = 2395.2 × 10^{-4} $cm^{-1}$and |E| = 4.2E-13 × 10^{-4} cm^{-1} for center I. For symmetry that is orthorhombic, the ratio b_2^2/b_2^0 should fall between 0 and 1 [33]. In the current calculation, the ratio $|b_2^2|/|b_2^0|$ = 5.2E-16 and |E| / |D| = 1.74E-16 for the center I. It is seen that the calculated values of |D| and |E| do not match with the experimental ones though $|b_2^2|/|b_2^0|$ falls in the specified range [33]. Therefore, with the above t_2 and reference distance R_0, the ZFS parameters |D| and |E| are calculated for Cr^{3+} at the Sn^{4+} site with distortion having position Sn^{4+} (-0.1662, -0.1185, -0.0022) for center I. The local environment about Cr^{3+} is shown in Figure 2. The traditional ZFS parameters obtained now are |*D*| = 5778.1 × 10^{-4} cm^{-1}, |*E*| = 953.6 × 10^{-4} $cm^{-1}$for center I, which are matching fairly well with the values found from the experiment. The ratio $|b_2^2|/|b_2^0|$ = 0.495 and |*E*| / |*D*| = 0.165 for the center I are in the specified range [34]. Further, with the above t_2 and reference distance R_0, the ZFS parameters |*D*| and |*E*| are calculated for Cr^{3+} at the interstitial site but the values discovered differ significantly from the experimental ones. For this reason, they are not included here.

Table 2 gives the experimental and calculated ZFS parameters of the Cr^{3+} ion in SnO_2. It shows that the ZFS parameters |D| and |E| are in fair agreement with the values of the experiment [17] when the distortion is introduced into the calculation.

Computations of the crystal field's parameters

The transition ion CF energy states in crystals [34-37] can be obtained using Wybourne operators as follows [19,38,39]:

$$H_{CF} = \sum_{kq} B_{kq} C_q^{(k)} \quad (6)$$

Where H_{CF} is CF Hamiltonian. The metal-ligand complex's CF parameters in equation (6) are found using SPM [24,25] as follows:

$$\mathcal{B}_{kq} = \sum_i \bar{A}k\left(\frac{R_0}{Ri}\right)^{tk} K_{kq}\left(\theta_i, \varphi_i\right) \quad (7)$$

R_0 denotes the reference distance, R_i, θ_i, φ_i provide the i^{th}

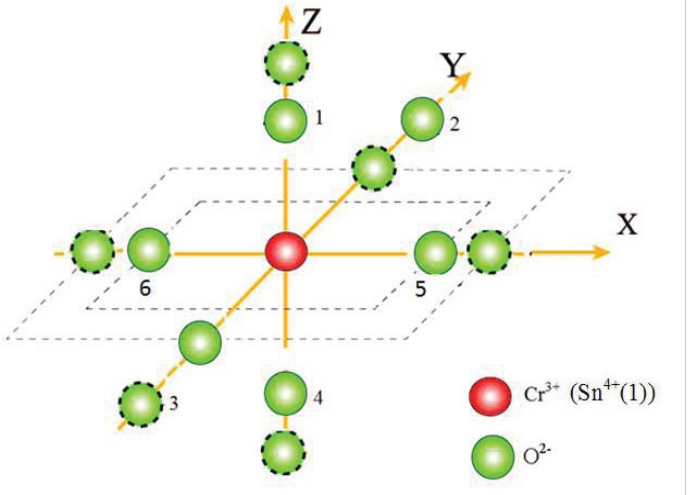

Figure 2: Visual depiction of the local environment (dotted circles show positions after distortion).

Table 2: The reference distance and calculated and Cr^{3+}'s experimental ZFS parameters in a single crystal of SnO_2 for the center I.

Site	R_0 Å	Calculated ZFS parameters (cm^{-1}) parameters ($10^{-4}cm^{-1}$)			Conventional ZFS		
		$\|b_2^0\|$	$\|b_2^2\|$	$\|b_2^2\|/\|b_2^0\|$	$\|D\|$	$\|E\|$	$\|E\|/\|D\|$
ND Center I	2.00	0.23953	1.2E-16	5.2E-16	2395.2	4.2E-13	1.74E-16
WD	2.00	0.57781	0.28607	0.495	5778.1	953.6	0.165
					5778.2[e]	2785.5[e]	0.482

WD = With Distortion; ND = No Distortion, E = Experimental.

ISSN 2995-8067 DOI: 10.61927/igmin207

ligand spherical polar coordinates and K_{kq} are the coordination factors [34]. $\bar{A}_2$ = 40, 400 cm^{-1}, t_2 = 1.3, $\bar{A}_4$ =11, 700 cm^{-1} and t_4 = 3.4 are used to find B_{kq} (k = 2, 4; q = 0, 2, 4) [34]. Table 3 contains a list of the calculated B_{kq} parameters. The ratio $|B_{22}|/|B_{20}|$ = 0.091 for the center I, which suggests that B_{kq} parameters established are standardized [33]. In order to analyze the optical spectroscopy data using the crystal-field approach, an efficient computer program for diagonalization of a complete Hamiltonian (including electrostatic terms, Trees correction, spin-orbit interaction, and crystal-field) within the $3d^N$ configuration (N = 2 to 8) is essential. Yeung and Rudowicz [35,36] recently developed a computer program CFA for $3d^N$ configuration (N = 2 to 8) and for symmetry as low as orthorhombic. The CF analysis computer program is suitable for orthorhombic symmetry, tetragonal symmetry, cubic symmetry, trigonal symmetry, and hexagonal symmetry. Monoclinic and triclinic as well as trigonal and tetragonal symmetry cases involving "imaginary" CF terms are also included. Note that in the latter cases, the complex CF parameter can be made real by an appropriate rotation around the z-axis. Other low-spin states, e.g. S = 1, 0, for $3d^4$ and $3d^6$ ions and S = 3/2, l/2 for $3d^5$ ions, arising at strong ligand fields, as well as the low spin to high spin transition can also be studied using the package. The Hamiltonian for a $3d^N$ ion in crystals can be written as the sum of the free-ion Hamiltonian, the spin-orbit interaction, and the Trees correction describing the two body orbit-orbit polarization. The crystal (ligand) field Hamiltonian in the equation in Wybourne's notation is taken in terms of the crystal field parameters B_{kq} and the renormalized spherical tensor operators. Since the ligand field is in the weak to intermediate range for most of the 3d transition metal ions in crystals, the basis of states in the LS coupling scheme can be taken. The Slater integrals F^k (k = 0, 2, and 4) are related to the Racah parameters *A, B,* and C as follows:

$$A=F_0-49F_4$$

$$B = F_2 - 5F_4$$

$$C = 35F_4$$

And $F_0 = F^0$, $F_2 = F^2/49$, $F_4 = F^4/441$. Usually, we set A = 0 since it will cause no energy

Level splittings apart from shifting the center of the whole spectrum. Racah parameters A, B, C, Tree's correction and spin-orbit coupling, and the CF parameters B_{kq} are taken as input parameters.

The total Hamiltonian is diagonalized to calculate the CF energy levels of the Cr^{3+} ion in SnO_2 single crystals using the B_{kq} parameters in Table 3 and the CFA computer program [35,36]. Table 4 shows the energy values that were calculated. The calculated and experimental energy values for Cr^{3+}: Cassiterite (SnO_2) [40] are contrasted. The experimental and theoretical energy values seem to be reasonably in agreement based on Table 4. Therefore, the experimental findings are supported by examining Cr^{3+} ions at Sn^{4+} sites in SnO_2 theoretically [17,40].

Table 3: B_{kq} parameters of Cr^{3+} for center I with distortion in a single crystal of SnO_2.

Calculated B_{kq} (cm^{-1}) Parameters used for the CFA program							
Site	R0Å	B_{20}	B_{22}	B_{40}	B_{42}	B_{44}	$\lvert B_{22}\rvert / \lvert B_{20}\rvert$
Center I WD	2	-86000.9	-7869.12	46442.65	10243.45	-94402.8	0.091

WD = With Distortion.

Table 4: Energy values of Cr^{3+} in SnO_2 single crystal determined by computation and experimentation (center I).

Transition from	Observed	Calculated band using CFA (cm^{-1})
$^4A_{2g}(F)$	band (cm^{-1})	Center I
$^2E_g(G)$	14518	12396, 12533
$^2T_{1g}(G)$		12669, 13605, 14076
$^4T_{2g}(F)$	18389	14735, 14800, 15282,15414, 15897, 20316
$^4T_ig(F)$	23228	24334, 26120, 27018,27597, 27897, 28835
$^4T_{1g}(P)$		29673, 30762, 30961,31575, 42777, 46856
$^2T_{1g}(aD)$		49768, 52745, 79331
$^2E_g(bD)$		79342, 83419

(The spin-orbit coupling constant, the Racah parameters A, B, and C, and the Trees correction have respective values of 276, 0, 442, 3676, and 70 cm^{-1}).

SPM studies of $3d^N$ ions in ferroelectrics, for example, Fe^{3+} ions in $PbZrO_3$, $Pb(Zr_xTi_{1-x})O_3$ and $PbTiO_3$ and Cr^{3+} ions in $PbTiO_3$ and $Ba_xPb_{1-x}TiO_3$ powders, Mn^{2+} ions in $BaTiO_3$ nanopowders, and other related ion-host systems as well as Fe^{3+} and Mn^{2+} in ZnO also back the experimental EPR findings [8]. The major usage of this investigation may be done in studies of Single Molecule Magnets (SMM), Single-Chain Magnets (SCM), and Single Ion Magnets (SIM) based on transition ions for computational modeling of their properties. The SMM, SCM, and SIM are formed by polynuclear clusters assembled from mononuclear coordination complexes. These systems have become a subject of large interest due to their unique magnetic properties like the phenomenon of macroscopic quantum tunneling of magnetization, as well as possible applications in high-density information storage and quantum computing [8]. Recently many novel SMM or SCM systems containing Cr^{3+} and/or Mn^{2+} ions as well as nanomagnets with elaborate coordination geometry containing Gd^{3+} ions have been synthesized [8].

The spectra of optical absorption of Cr^{3+}-activated phosphors are now explained using Franck-Condon analysis using the model known as configurational-coordinate (CC) [41]. The various excited state-ground state transitions in Cr^{3+} are a result of the lattice vibrations' strong coupling (CC model) [41]. The CC model is not being utilized so there is a difference between excited-state peak energies obtained here and energies of the zero-phonon line (ZPL) discussed in [41,42]. There are two types of oxide-phosphors that are doped with Cr^{3+}: the O-Cr-A type and the O-Cr-B type. The characteristics

of type O-Cr-A phosphors' luminescence are obtained from the ^2E_g-related luminescence transitions as their crystal-field strength lies in the region of Dq/B > 2.1 while type O–Cr–B phosphors have a crystal-field strength falling within the range of Dq/B < 2.1, as a result, the transitions associated with $^4T_{2g}$ are used to find their luminescence properties. SnO_2: Cr^{3+} is classified as an O-Cr-A type phosphor (Dq/B = 4.15, > 2.1) [42].

Summary and conclusion

The Crystal Field (CF) and Zero-Field Splitting (ZFS) parameters for Cr^{3+} ions in SnO_2 single crystals are determined using the Superposition Model (SPM). Calculations are performed using the interstitial site, distortion models, and Cr^{3+} ions in SnO_2 crystal at Sn^{4+} ion sites. When distortion is included in the calculation, the calculated conventional ZFS values for the Cr^{3+} ion at Sn^{4+} sites in SnO_2 single crystal give a reasonable accord with the experimental values. It is found that the Cr^{3+} ions in the SnO_2 lattice replace the Sn^{4+} ions at those locations. The CF energy values for Cr^{3+} ions at Sn^{4+} sites calculated with CF parameters and the CFA program show an adequate degree of conformity with the experimental ones. Therefore, the theoretical inferences support the experimental result.

The modeling approach adopted in this work could prove useful in the future to find crystals for different industrial and scientific applications by correlating EPR and optical data for several other ion-host systems. The major usage of this investigation may be done in studies of Single Molecule Magnets (SMM), Single-Chain Magnets (SCM), and Single Ion Magnets (SIM) based on transition ions for computational modeling of their properties.

Acknowledgement

The CFA computer program was provided by Prof. C. Rudowicz of the Chemistry Faculty at A. Mickiewicz University in Poznan, Poland, for which the authors are grateful, and the department head of physics for the departmental facilities.

References

1. Stefaniuk I, Rudowicz C, Gnutek P, Suchocki A. EPR Study of Cr3+ and Fe3+ Impurity Ions in Nominally Pure and Co2+-Doped YAlO3 Single Crystals. Appl Magn Reson. 2009;36:371-380.
2. Mabbs FE, Collison D, Gatteschi D. Electron Paramagnetic Resonance of d Transition Metal Compounds. Amsterdam: Elsevier; 1992.
3. Weil JA, Bolton JR. Electron Paramagnetic Resonance: Elementary Theory and Practical Applications. 2nd ed. New York: Wiley; 2007.
4. Pilbrow JR. Transition Ion Electron Paramagnetic Resonance. Oxford: Clarendon Press; 1990.
5. Bansal RS, Seth VP, Chand P, Gupta SK. EPR and optical spectra of vanadyl ion (impurities) in three polycrystalline solids. J Phys Chem Solids. 1991;52:389-392.
6. Brik MG, Avram CN, Avram NM. Calculations of spin Hamiltonian parameters and analysis of trigonal distortions in LiSr(Al,Ga)F6+ crystals. Physica B. 2006;384:78-81. doi: 10.1016/j.physb.2006.05.155.
7. Pandey S, Kripal R, Yadav AK, Açıkgöz M, Gnutek P, Rudowicz C. Implications of direct conversions of crystal field parameters into zero-field splitting ones - Case study: Superposition model analysis for Cr3+ ions at orthorhombic sites in LiKSO4. J Lumin. 2021;230:117548.
8. Rudowicz C, Gnutek P, Açikgöz M. Superposition model in electron magnetic resonance spectroscopy – a primer for experimentalists with illustrative applications and literature database. Appl Spectr Rev. 2019;54(8):673-718. https://doi.org/10.1080/05704928.2018.1494601.
9. Shehzad K, Shah NA, Amin M, Abbas M, Syed WA. Synthesis of SnO2 Nanowires for CO, CH4 and CH3OH Gases Sensing. Int J Distrib Sens Netw. 2018;14(8):1-10. https://doi.org/10.1177/1550147718790750.
10. Lee SG, Han SB, Lee WJ, Park KW. Effect of Sb-Doped SnO2 Nanostructures on Electrocatalytic Performance of a Pt Catalyst for Methanol Oxidation Reaction. Catalysts. 2020;10(8):2-15. https://doi.org/10.3390/catal10080866.
11. Dinh NN, Bernard MC, Goff AH, Stergiopoulos T, Falaras P. Photoelectrochemical Solar Cells Based on SnO2 Nanocrystalline Films. CR Chim. 2006;9(5-6):676-683. https://doi.org/10.1016/j.crci.2005.02.042.
12. Manikandan K, Dhanuskodi S, Maheswari N, Muralidharan G. SnO2 Nanoparticles for Supercapacitor Application. AIP Conf Proc. 2016; 173:050048. http://dx.doi.org/10.1063.4947702.
13. Ginley DS. Transparent Conducting Oxides Based on Tin Oxide. In: Kykyneshi R, Zeng JP, Cann DP, eds. Handbook of Transparent Conductors. 2011:171-191. http://dx.doi.org/10.1007/978-1-4419-1638-96.
14. Bhawna, Choudhary AK, Gupta A, Kumar S, Kumar P, Singh RP, Kumar V. Synthesis, Antimicrobial Activity, and Photocatalytic Performance of Ce Doped SnO2 Nanoparticles. Front Nanosci. 2020;2:595352. http://dx.doi.org/10.3389/fnano.2020.595352.
15. Filippatos PP, Kelaidis N, Vasilopoulou M, Davazoglou D, Chroneos A. Defect Processes in Halogen Doped SnO2. Appl Sci. 2021;11(2):1-14. https://doi.org/10.3390/app11020551.
16. Loan TT, Huong VH. Characterizations of Cr3+-doped SnO2 Powders Via a Hydrolysis Method. VNU J Sci: Math - Phys. 2023;39(4):55-63.
17. From WH. Electron paramagnetic Resonance of Cr3+ in SnO2. Phys Rev. 1963;131:961-963.
18. Von Werner HB. Uber die Verfeinerung der Kristallstrukturbestimmung einiger Vertreter des Rutiltyps: TiO2, SnO2, GeO2 und MgF2. Acta Cryst. 1956;9:515-520.
19. Rudowicz C, Karbowiak M. Disentangling intricate web of interrelated notions at the interface between the physical (crystal field) Hamiltonians and the effective (spin) Hamiltonians. Coord Chem Rev. 2015;287:28-63.
20. Rudowicz C. Concept of spin Hamiltonian, forms of zero field splitting and electronic Zeeman Hamiltonians and relations between parameters used in EPR. A critical review. Magn Reson Rev. 1987;13:1-89. Erratum, Rudowicz C. Magn Reson Rev. 1988;13:335.
21. Rudowicz C, Misra SK. Spin-Hamiltonian formalisms in electron magnetic resonance (EMR) and related spectroscopies. Appl Spectrosc Rev. 2001;36(1):11-63.
22. Rudowicz C. Transformation relations for the conventional Okq and normalised O'kq Stevens operator equivalents with k=1 to 6 and –k ≤ q ≤ k. J Phys C Solid State Phys. 1985;18(7):1415-1430; Erratum: Rudowicz C. J Phys C Solid State Phys. 1985;18(19):3837.
23. Rudowicz C, Chung CY. The generalization of the extended Stevens operators to higher ranks and spins, and a systematic review of the tables of the tensor operators and their matrix elements. J Phys Condens Matter. 2004;16(32):5825-5847.

24. Newman DJ, Ng B, eds. Superposition model. In: Newman DJ, Ng B, eds. Crystal Field Handbook. UK: Cambridge University Press; 2000:83-119.

25. Newman DJ, Ng B. The Superposition model of crystal fields. Rep Prog Phys. 1989;52:699-763.

26. Rudowicz C. On the derivation of the superposition-model formulae using the transformation relations for the Stevens operators. J Phys C Solid State Phys. 1987;20(35):6033-6037.

27. Rudowicz C, Gnutek P, Açıkgöz M. Superposition model in electron magnetic resonance spectroscopy – a primer for experimentalists with illustrative applications and literature database. Appl Spectrosc Rev. 2019;54:673-718.

28. Açıkgöz M. A study of the impurity structure for 3d3 (Cr3+ and Mn4+) ions doped into rutile TiO2 crystal. Spectrochim Acta A Mol Biomol Spectrosc. 2012 Feb;86:417-22. doi: 10.1016/j.saa.2011.10.061. Epub 2011 Nov 7. PMID: 22112572.

29. Müller KA, Berlinger W, Albers J. Paramagnetic resonance and local position of Cr3+ in ferroelectric BaTiO3. Phys Rev B Condens Matter. 1985 Nov 1;32(9):5837-5844. doi: 10.1103/physrevb.32.5837. PMID: 9937831.

30. Müller KA, Berlinger W. Superposition model for sixfold-coordinated Cr^{3+} in oxide crystals (EPR study). J. Phys. C: Solid State Phys. 1983; 16(35): 6861-6874.

31. Yeom TH, Chang YM, Rudowicz C. Cr^{3+} centres in $LiNbO_3$: Experimental and theoretical investigation of spin Hamiltonian parameters. Solid State Commun. 1993; 87(3): 245-249.

32. Siegel E, Muller K A. Structure of transition-metal—oxygen-vacancy pair centers. Phys. Rev. B 1979; 19(1): 109-120.

33. Rudowicz C, Bramley R. On standardization of the spin Hamiltonian and the ligand field Hamiltonian for orthorhombic symmetry. J. Chem. Phys. 1985; 83(10): 5192-5197.

34. Yeung YY, Newman DJ. Superposition-model analyses for the Cr3+ 4A2 ground state. Phys Rev B Condens Matter. 1986 Aug 15;34(4):2258-2265. doi: 10.1103/physrevb.34.2258. PMID: 9939914.

35. Yeung YY, Rudowicz C. Ligand field analysis of the $3d^N$ ions at orthorhombic or higher symmetry sites. Comp. Chem. 1992; 16(3): 207-216.

36. Yeung YY, Rudowicz C. Crystal Field Energy Levels and State Vectors for the $3d^N$ Ions at Orthorhombic or Higher Symmetry Sites. J. Comput. Phys. 1993;109(1): 150-152.

37. Chang Y M, Rudowicz C, Yeung YY. Crystal field analysis of the $3d^N$ ions at low symmetry sites including the 'imaginary' terms. Computers in Physics 1994; 8(5**):** 583-588.

38. Wybourne BG. Spectroscopic Properties of Rare Earth. New York, USA: Wiley; 1965.

39. Figgis BN, Hitchman MA. Ligand Field Theory and its Applications. New York: Wiley; 2000.

40. Adekeye JID. Optical Absorption Spectra of Chromium in Cassiterite Single Crystals. J Am Sci. 2009;5(4):141-146.

41. Adachi S. Photoluminescence Spectroscopy and Crystal-Field Parameters of Cr3+ Ion in Red and Deep Red-Emitting Phosphors. ECS J Solid State Sci Tech. 2019;8(12).

42. Adachi S. Review—Photoluminescence Properties of Cr3+-Activated Oxide Phosphors. ECS J Solid State Sci Tech. 2021;10:026001.

How to cite this article: Bharati M, Singh V, Kripal R. Modeling of Cr^{3+} doped Cassiterite (SnO_2) Single Crystals. IgMin Res. June 28, 2024; 2(6): 484-489. IgMin ID: igmin207; DOI: 10.61927/igmin207; Available at: igmin.link/p207